Systematic modeling-driven experiments identify distinct molecular clockworks underlying hierarchically organized pacemaker neurons

Eui Min Jeong[a,b,1], Miri Kwon[c,d,1], Eunjoo Cho[c,d,1], Sang Hyuk Lee[c,d], Hyun Kim[b], Eun Young Kim (김은영)[c,d,2], and Jae Kyoung Kim[a,b,2]

[a]Department of Mathematical Sciences, Korea Advanced Institute of Science and Technology, Daejeon 34141, Republic of Korea; [b]Biomedical Mathematics Group, Institute for Basic Science, Daejeon 34126, Republic of Korea; [c]Department of Biomedical Sciences, Ajou University Graduate School of Medicine, Kyunggi-do 16499, Republic of Korea; and [d]Department of Brain Science, Ajou University School of Medicine, Kyunggi-do 16499, Republic of Korea

Edited by Joseph Takahashi, HHMI and Department of Neuroscience, The University of Texas Southwestern Medical Center, Dallas, TX; received July 20, 2021; accepted January 18, 2022

In metazoan organisms, circadian (~24 h) rhythms are regulated by pacemaker neurons organized in a master–slave hierarchy. Although it is widely accepted that master pacemakers and slave oscillators generate rhythms via an identical negative feedback loop of transcription factor CLOCK (CLK) and repressor PERIOD (PER), their different roles imply heterogeneity in their molecular clockworks. Indeed, in *Drosophila*, defective binding between CLK and PER disrupts molecular rhythms in the master pacemakers, small ventral lateral neurons (sLN_vs), but not in the slave oscillator, posterior dorsal neuron 1s ($DN1_ps$). Here, we develop a systematic and expandable approach that unbiasedly searches the source of the heterogeneity in molecular clockworks from time-series data. In combination with in vivo experiments, we find that sLN_vs exhibit higher synthesis and turnover of PER and lower CLK levels than $DN1_ps$. Importantly, light shift analysis reveals that due to such a distinct molecular clockwork, sLN_vs can obtain paradoxical characteristics as the master pacemaker, generating strong rhythms that are also flexibly adjustable to environmental changes. Our results identify the different characteristics of molecular clockworks of pacemaker neurons that underlie hierarchical multi-oscillator structure to ensure the rhythmic fitness of the organism.

circadian rhythms | CLOCK | dorsal neuron | lateral neuron | mathematical modeling

The circadian clock enables organisms to manifest about 24-h (circadian) rhythms of behavior and physiology coordinated with rhythmic environmental changes. The generic model of the circadian clock is composed of input, oscillator, and output, wherein the oscillator entrains to time cues (zeitgeber) and regulates the output rhythms (1, 2). This system operates as a network in which the master pacemaker and slave oscillator are organized in a hierarchical manner (3–6). The master pacemaker receives the light signal, the prominent zeitgeber, and then drives the slave oscillator that regulates distinct outputs such as sleep, feeding, metabolic homeostasis, etc. (3–6). In this hierarchy system, the master pacemaker can generate strong rhythms to yield clear signals to the slave oscillator while still being able to flexibly adjust their phase in response to changes in environmental lighting conditions. However, the molecular mechanisms underlying these somewhat paradoxical characteristics of the master pacemaker are poorly understood.

In *Drosophila*, small ventral lateral neurons (sLN_vs) act as the master pacemaker. That is, sLN_vs maintain free-running rhythms under constant darkness (7–9) and receive external light signals via the visual pathway (10–12). On the other hand, posterior dorsal neuron 1s ($DN1_ps$) act as the slave oscillator receiving neuropeptide pigment-dispersing factor (PDF) from sLN_vs, which is critical to maintain their rhythms (13–15). Without PDF signaling from sLN_vs, $DN1_ps$ rapidly lose molecular oscillation (13–15), and $DN1_ps$ follow the speed of genetically modified sLN_vs (5, 16). Furthermore, $DN1_ps$ harbor connections with output centers such as premotor, sleep, and neuroendocrine centers (17–22). Taken together, the circadian clock of *Drosophila* has a hierarchical organization, with sLN_vs being the master pacemaker receiving light signals and $DN1_ps$ being the slave oscillator releasing output signals, although the organization can be potentially changed in the presence of environmental or genetic perturbations (9, 23, 24).

Despite the different roles of these pacemaker neurons, they share common molecular mechanisms to generate circadian rhythms that are well conserved in all life-forms: the interlocked multiple transcriptional-translational feedback loops (TTFLs) composed of core clock proteins (25, 26). In the *Drosophila* core TTFL, CLK, and CYCLE (CYC) activate the transcription of *per* and *timeless* (*tim*); PER and TIM proteins, in turn, repress their own transcription in which PER is the core repressor. This core TTFL regulates the 24-h period rhythmic expression of clock genes and other clock-controlled genes.

Significance

The hierarchically organized master and slave clock neurons are widely believed to generate circadian rhythms via an identical molecular clockwork. However, their different roles in regulating those rhythms raise the question of whether their molecular clockworks differ. Here, leveraging systematic model-driven in vivo experiments for an unbiased search for their heterogeneity, we found that the master clock neurons have higher synthesis and turnover rates of repressor and lower activator levels than the slave clock neurons. Further in silico analysis revealed that this distinguished molecular clockwork of the master clock neurons allows them to generate strong rhythms but also to flexibly adjust rhythms upon environmental perturbation. This explains how the circadian clock can have two contradictory properties, robustness and flexibility.

Author contributions: E.C., E.Y.K., and J.K.K. designed research; E.M.J., M.K., E.C., S.H.L., E.Y.K., and J.K.K. performed research; E.M.J., M.K., E.C., S.H.L., H.K., E.Y.K., and J.K.K. analyzed data; and E.M.J., M.K., E.C., S.H.L., H.K., E.Y.K., and J.K.K. wrote the paper.

The authors declare no competing interest.

This article is a PNAS Direct Submission.

[1]E.M.J., M.K., and E.C. contributed equally to this work.

[2]To whom correspondence may be addressed. Email: ekim@ajou.ac.kr or jaekkim@kaist.ac.kr.

This article contains supporting information online at http://www.pnas.org/lookup/suppl/doi:10.1073/pnas.2113403119/-/DCSupplemental.

Published February 22, 2022.

Although sLN_vs and $DN1_ps$ generate circadian rhythms via identical TTFLs, unexpectedly, we previously found that their rhythms are altered in a different way in p{*Clk*-Δ};Clk^{out} flies (here referred to as *Clk*-Δ flies), which express CLK defective in PER binding (27). Specifically, in *Clk*-Δ flies, PER oscillation was significantly dampened in sLN_vs but quasinormal in $DN1_ps$, demonstrating heterogeneity in their molecular clocks.

Here, we took advantage of *Clk*-Δ flies to understand pacemaker neuron–specific molecular clockworks. Specifically, we analyzed the neuron-specific alteration of a time series of PER in *Clk*-Δ flies by developing a systematic modeling approach. This allowed us to systematically investigate all possible molecular differences in the core TTFL between sLN_vs and $DN1_ps$ with their mathematical models developed in this study. With a combination of in vivo experiments, we found essential differences in the molecular clockworks of sLN_vs and $DN1_ps$ to reproduce their different rhythm alterations by *Clk*-Δ: CLK levels are higher in $DN1_ps$ than in sLN_vs, the synthesis of PER is more efficient, and the degradation of PER is faster in sLN_vs than in $DN1_ps$. Furthermore, we found that such distinct molecular mechanisms of the core TTFL in sLN_vs are critical for its ability to act as the master pacemaker, generating strong rhythms while flexibly adapting its phase to environmental changes (e.g., jet lag) via in silico experiments. In conclusion, our study presents pacemaker neuron–specific molecular clockworks that underlie the hierarchical organization of the circadian clock to ensure the rhythmic fitness of the organism.

Results

PER Rhythms Are Dampened in sLN_vs but Not in $DN1_ps$ in *Clk*-Δ Flies. CLK-Δ is a deletion mutant of CLK lacking amino acids (AA) 657 through 707, which are crucial for interaction with PER, and thus is defective in PER binding (Fig. 1*A*) (27). Because PER binding–induced hyperphosphorylation and subsequent degradation is less likely to occur for CLK-Δ compared to CLK-WT, CLK-Δ is more stable than CLK-WT (Fig. 1*A*) (27). Furthermore, CLK-Δ has lower transcriptional activity compared to CLK-WT (27), which appears to be due to impaired interaction with the E-box (CACGTG) of the *per* gene, as shown with mouse CLK lacking exon 19 (homologous to AA 657 through 707) (Fig. 1*A*) (28).

Due to these biochemical deficits of CLK-Δ compared to CLK-WT, *Clk*-Δ flies exhibit altered molecular rhythms compared to control *Clk*-WT flies. Previously, we reported that the molecular rhythms of different pacemaker neurons in the brain (Fig. 1*B*) are differentially altered by the CLK-Δ mutation. Specifically, PER levels are more strongly reduced in LN_vs than in $DN1_ps$ of *Clk*-Δ flies compared to *Clk*-WT flies (27). PER levels throughout the light–dark (LD) cycle were requantitated with the data from the previous report, and their amplitudes were calculated (Fig. 1 *C* and *D* and *SI Appendix*, Table S1). While the amplitude is reduced by about 50% in sLN_vs of *Clk*-Δ flies compared to *Clk*-WT flies, the amplitudes of the PER rhythms are maintained in $DN1_ps$ of *Clk*-Δ flies (Fig. 1*D*). We then measured PER rhythms in constant dark condition (DD) (Fig. 1*E*), which showed a more dramatic difference between sLN_vs and $DN1_ps$. Specifically in sLN_vs, PER rhythms are abolished in *Clk*-Δ flies (*SI Appendix*, Table S1), which is consistent with their arrhythmic behavior under DD (27). $DN1_ps$ of *Clk*-Δ flies show intact rhythms, albeit peak and trough levels are reduced compared to control flies. Consistently, the amplitudes of the PER rhythms in sLN_vs of *Clk*-Δ flies are greatly reduced compared to those of *Clk*-WT flies but not in $DN1_ps$ of *Clk*-Δ flies (Fig. 1*F*). These different effects of the CLK-Δ mutation on PER rhythms in sLN_vs or $DN1_ps$ imply that their core TTFL might be different.

Mathematical Modeling Predicts Differences in Molecular Clockworks between sLN_vs and $DN1_ps$. To identify the differences in molecular clockworks between two pacemaker neurons, we developed a mathematical model describing the core TTFL of the circadian clock in sLN_vs and $DN1_ps$ (Fig. 2 *A*, *Top*; see *SI Appendix* for details). In the model, CLK binds to the E-box of the *per* promoter and activates the transcription of *per* messenger RNA (mRNA). Next, *per* mRNA is translated to PER in the cytoplasm and then enters the nucleus, where it inhibits CLK by forming a 1:1 stoichiometric complex with CLK. For simplicity, CYC and TIM are not considered in the model. Thus, light, which destabilizes cytoplasmic TIM, is assumed to directly destabilize cytoplasmic PER, because TIM stabilizes PER (*SI Appendix*, Fig. S1) (29–32).

Next, we unbiasedly searched parameters of the model to simulate the different time series of PER between sLN_vs and $DN1_ps$ (Fig. 1 *C*–*F*) by developing a systematic modeling approach (*SI Appendix*, Fig. S2). Specifically, to investigate all possible differences in the core TTFL between sLN_vs and $DN1_ps$ without bias, we allowed that the parameters of their models, which are referred to as LN and DN models, can differ, except for dissociation constants between molecules (Fig. 2 *A*, *Middle*; red and blue triangles represent a set of model parameters for sLN_vs and $DN1_ps$, respectively). Furthermore, to construct LN-Δ and DN-Δ models by switching CLK-WT to CLK-Δ in the LN and DN models, respectively, we allowed larger CLK levels and higher dissociation constants between PER and CLK, between PER and CLK:E-box, and between CLK and E-box, compared to CLK-WT, reflecting the experimental data (Fig. 1*A*) (27, 28). The parameters of the LN, DN, LN-Δ, and DN-Δ models were estimated together by fitting them to the eight time-series data of PER for sLN_vs of *Clk*-WT flies, sLN_vs of *Clk*-Δ flies, $DN1_ps$ of *Clk*-WT flies, and $DN1_ps$ of *Clk*-Δ flies under LD and DD with the simulated annealing (SA) algorithm (Fig. 2 *A*, *Bottom*). During the fitting, to avoid unnecessary differences among these four models, we used a regularization cost penalizing the difference in the values of parameters between the LN and DN models as well as the fitting cost (*SI Appendix*, Fig. S2 B and D; see *SI Appendix* for details).

In this way, we found 10^3 parameter sets with which the four models can successfully reproduce the experimentally observed time series with minimal differences between the LN and DN models (Fig. 2*B*, *SI Appendix*, Fig. S3, and Dataset S1). In particular, the simulated time series successfully captured the dampened rhythms in sLN_vs of *Clk*-Δ flies and quasinormal rhythms in $DN1_ps$ of *Clk*-Δ flies. Next, we investigated the 10^3 parameter sets to identify key differences between the LN and DN models. Interestingly, we found that the parameters describing the degradation and synthesis rates of PER were greater in the LN model than in the DN model, while the parameter describing the CLK level was lower in the LN model than in the DN model (Fig. 2*C*). On the other hand, there were no apparent differences between the LN and DN models in parameters describing the nuclear translocation of PER (Fig. 2*C*) and the light-induced change of PER degradation (*SI Appendix*, Fig. S4). This predicts that CLK levels in sLN_vs are lower compared to $DN1_ps$ and that the synthesis and degradation rates of PER in sLN_vs are higher compared to $DN1_ps$ (Fig. 2*D*). The higher synthesis and degradation rates of sLN_vs lead to larger amplitudes compared to $DN1_ps$ (33). Importantly, due to the higher synthesis rates and lower CLK levels, the transcription of the LN model changes more sensitively in response to the change in the level of PER than the DN model, which is critical to generate stronger rhythms (*SI Appendix*, Fig. S5). However, due to the high sensitivity, when transcriptional repression of *per* is weakened by the weak binding affinity between CLK-Δ and PER, the LN model shows a more sensitive response compared to the DN model. That is, the molar

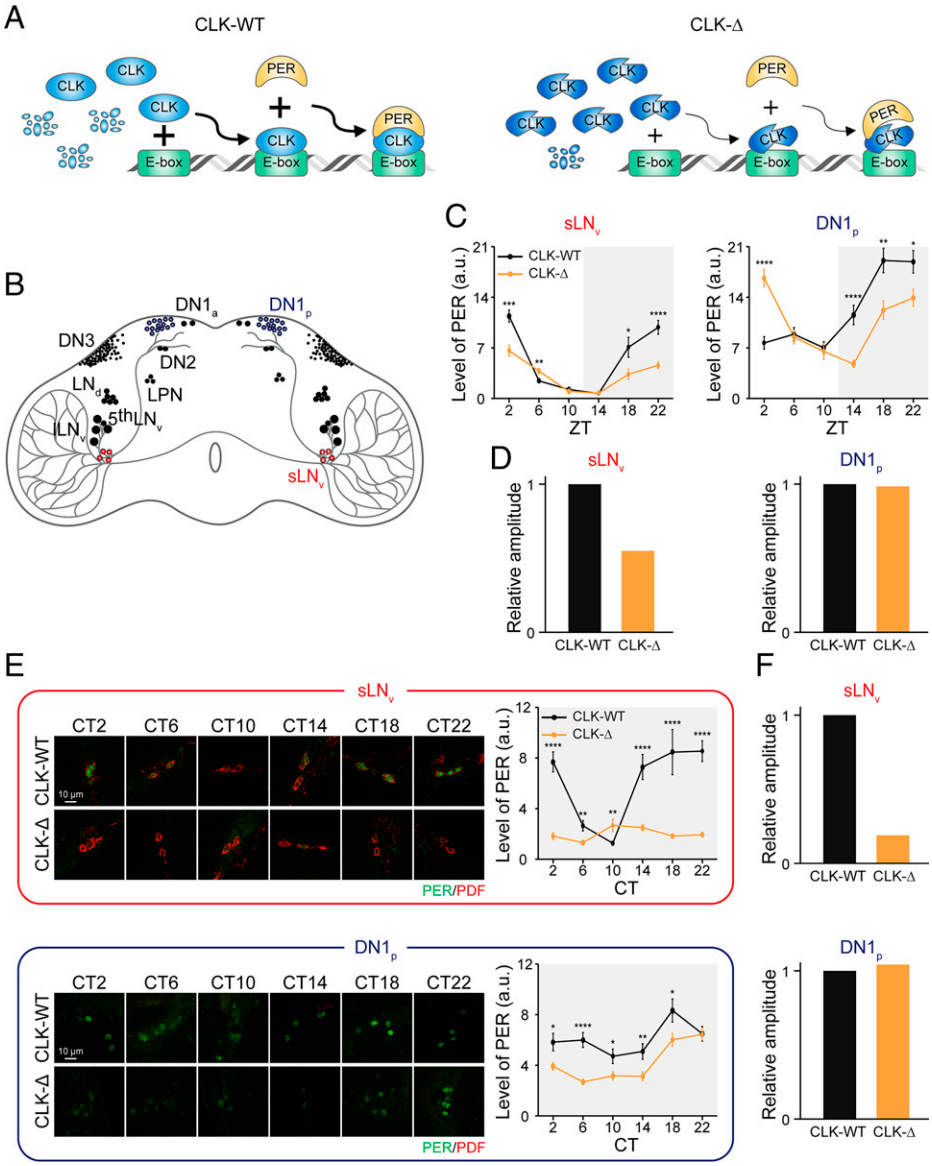

Fig. 1. Amplitudes of PER rhythms are reduced in sLN$_v$s, not in DN1$_p$s, of *Clk*-Δ flies under both LD and DD. (*A*) CLK-Δ has several biochemical deficits compared to CLK-WT. CLK-Δ is impaired in PER binding and E-box binding, leading to low E-box–dependent transcriptional activity. Furthermore, CLK-Δ is stable, so it presents in higher amounts than CLK-WT. (*B*) Schematic drawing of a *Drosophila* brain with pacemaker-neuron clusters. lLN$_v$, large ventral lateral neurons; sLN$_v$, small ventral lateral neurons; LN$_d$, dorsal lateral neurons; LPN, lateral posterior neurons; DN1–3, dorsal neuron groups 1 through 3; DN1$_a$, anterior DN1; DN1$_p$, posterior DN1. (*C*) PER levels in sLN$_v$s and DN1$_p$s throughout the LD cycle were requantitated with the data from the previous report by obtaining sum intensity of PER (see Materials and Methods for details) (25). White and gray backgrounds represent the L and D conditions, respectively. Values represent mean ± SEM; n = 24 to 50. Asterisks indicate a statistically significant difference between values at each time point (Student's t test; *P < 0.05, **P < 0.01, ***P < 0.001, ****P < 0.0001). The rhythmicities of all time series are significant according to the LR test (P < 0.01) (*SI Appendix*, Table S1). (*D*) Relative amplitudes of PER rhythms of *Clk*-WT (black) and *Clk*-Δ (orange) flies in *C*. The amplitudes of PER rhythms were normalized to that of *Clk*-WT flies. (*E*) *Clk*-WT and *Clk*-Δ flies were entrained under the LD cycle and kept in DD conditions. On the fourth day of DD, flies were collected at the indicated times and isolated brains were processed for whole-mount immunohistochemistry for PER (green) and PDF (red). PDF staining was used to mark LN$_v$s. Images are representative for each subset of pacemaker neurons. PER levels of sLN$_v$s and DN1$_p$s under DD conditions were quantified and values represent mean ± SEM; n = 24 to 41. Asterisks indicate a statistically significant difference between values at each time point (Student's t test; *P < 0.05, **P < 0.01, ****P < 0.0001). The rhythmicities of time series, except for sLN$_v$s of Clk-Δ flies, are significant according to the LR test (P < 0.01) (*SI Appendix*, Table S1). (*F*) Relative amplitudes of PER rhythms of *Clk*-WT and *Clk*-Δ flies in *E*, calculated as in *D*.

ratio between PER and CLK, which is critical for rhythm generation (34, 35), dramatically changes in sLN$_v$s, but not in DN1$_p$s, and results in the dampening of PER rhythms in sLN$_v$s but not in DN1$_p$s (*SI Appendix*, Fig. S5).

Verification of the Predicted Different Molecular Clockworks between sLN$_v$s and DN1$_p$s. We first examined CLK levels that were predicted by our model to be different in sLN$_v$s and DN1$_p$s (Fig. 2*C*). *Clk*-WT flies were entrained under a 12:12 LD cycle, and immunostaining of CLK was performed at ZT2 and ZT14, when transcriptional activity of CLK is low and high, respectively. We found that CLK levels in DN1$_p$s were higher compared to those in sLN$_v$s at both time points, which confirms the model prediction (Fig. 3 *A* and *B*).

Next, to validate whether the PER degradation rate is higher in sLN$_v$s than in DN1$_p$s, we performed cycloheximide (CHX) assays in vivo to block PER translation. Flies were transferred to CHX-containing food, and then PER degradation kinetics

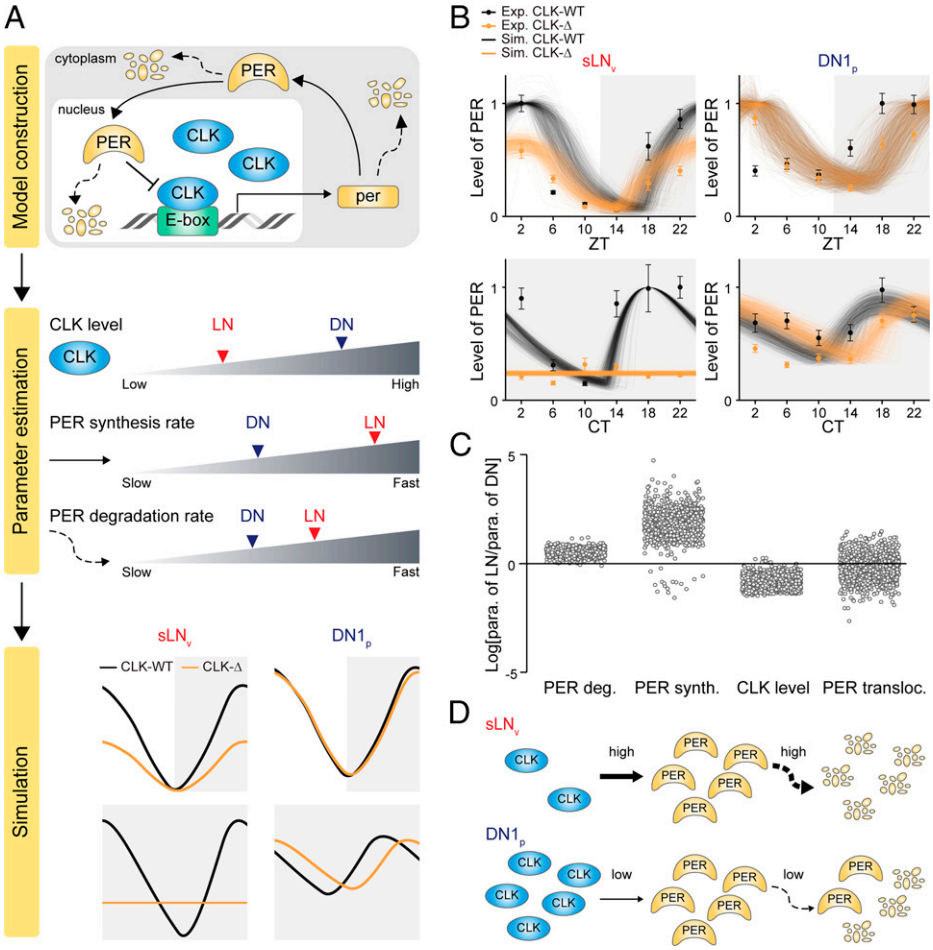

Fig. 2. A systematic modeling approach predicts differences in molecular clockworks between sLN$_v$s and DN1$_p$s. (*A*) A model diagram of a mathematical model describing the core TTFL in the *Drosophila* clock (*Top*). With this model, we investigated parameters describing differences in molecular clockworks between sLN$_v$s and DN1$_p$s (*Middle*) required to reproduce the time series of PER for sLN$_v$s of CLK-WT, sLN$_v$s of CLK-Δ, DN1$_p$s of CLK-WT, and DN1$_p$s of CLK-Δ under DD/LD (*Bottom*). Red and blue triangles represent a single set of model parameters for sLN$_v$s and DN1$_p$s, respectively. White and gray backgrounds represent the L and D conditions, respectively. (*B*) We repeated the parameter estimation until we obtained 10^3 successful parameter sets with which the models can reproduce the experimentally observed time series (dot). Both simulated and experimentally observed time series were normalized to their peak values. Here, white and gray backgrounds represent the L and D conditions, respectively. (*C*) The distributions of the log ratios between the parameters of the LN and DN models for PER degradation rates, PER synthesis rates, CLK levels, and PER nuclear translocation rates were obtained using the 10^3 parameter sets. To effectively compare the synthesis and decay of the total PER, we compared the multiplication of transcription and translation rates divided by the CLK level and the multiplication of the degradation rates of *per* mRNA, the cytoplasmic PER, and the nuclear PER, respectively. The log ratios of parameters describing degradation and synthesis of PER are predominantly positive, whereas the log ratios of parameters describing the CLK level are predominantly negative (Cohen's $d > 0.8$, indicating large effect size) (78). On the other hand, there are no apparent differences for the nuclear translocation rate of PER between LN and DN models (Cohen's $d < 0.5$, indicating small effect size) (78). Means (SDs) for the log ratios of degradation, synthesis, and the nuclear translocation rate of PER and CLK level are 0.5 (0.2), 1.7 (0.5), −0.2 (0.6), and −0.9 (0.3), respectively. (*D*) This predicts that the CLK levels in sLN$_v$s are lower than in DN1$_p$s, and the synthesis and degradation rates of PER in sLN$_v$s are higher than in DN1$_p$s.

were measured in each neuronal group. We first confirmed that the CHX treatment strategy worked by measuring PER levels every 1 h after CHX treatment beginning at CT15 when PER levels are low and PER synthesis begins. PER levels in sLN$_v$s and DN1$_p$s in the CHX-treated group did not increase, but those in the mock-treated group hugely increased (Fig. 3 *C* and *D*). Thus, CHX treatment effectively inhibited PER translation in flies. We next measured PER levels in sLN$_v$s and DN1$_p$s every 1 h after CHX treatment beginning at CT2 when PER levels are high and, thus, PER degradation mainly occurs. Indeed, PER in sLN$_v$s degraded much faster than PER in DN1$_p$s starting from CT2, which supports the model prediction (Fig. 3*E*).

PER synthesis was predicted to be much more efficient in sLN$_v$s than in DN1$_p$s (Fig. 2*C*). In fact, it has been reported that a complex containing TWENTY-FOUR (TYF) and ATAXIN-2 (ATX2) supports the translation of *per* mRNA in an LN-specific manner (36–38), which can lead to more efficient synthesis of PER in sLN$_v$s than DN1$_p$s. Nonetheless, this could not directly prove that the synthesis rate of PER is higher in sLN$_v$s than DN1$_p$s because there might be some other cell type–specific regulatory mechanism for synthesis. To examine whether the synthesis rate of PER is higher in sLN$_v$s than in DN1$_p$s, we tracked PER accumulation after 3 h of CHX treatment in each neuronal group. As the PER accumulation is regulated by both the synthesis and the degradation, minimizing the contribution of the degradation is necessary to translate the accumulation rate to the synthesis rate of PER. Thus, we used w*per*^{01};*per*ΔPDBD flies that are defective for Double Time (DBT) binding and thus are resistant to the degradation (39). Exposure of flies in CHX-containing food for 3 h greatly reduced PER levels to almost undetectable levels in sLN$_v$s and DN1$_p$s (Fig. 3 *F* and *G*). After the transfer of flies to normal food, the PER signal began to appear, and the rate of PER

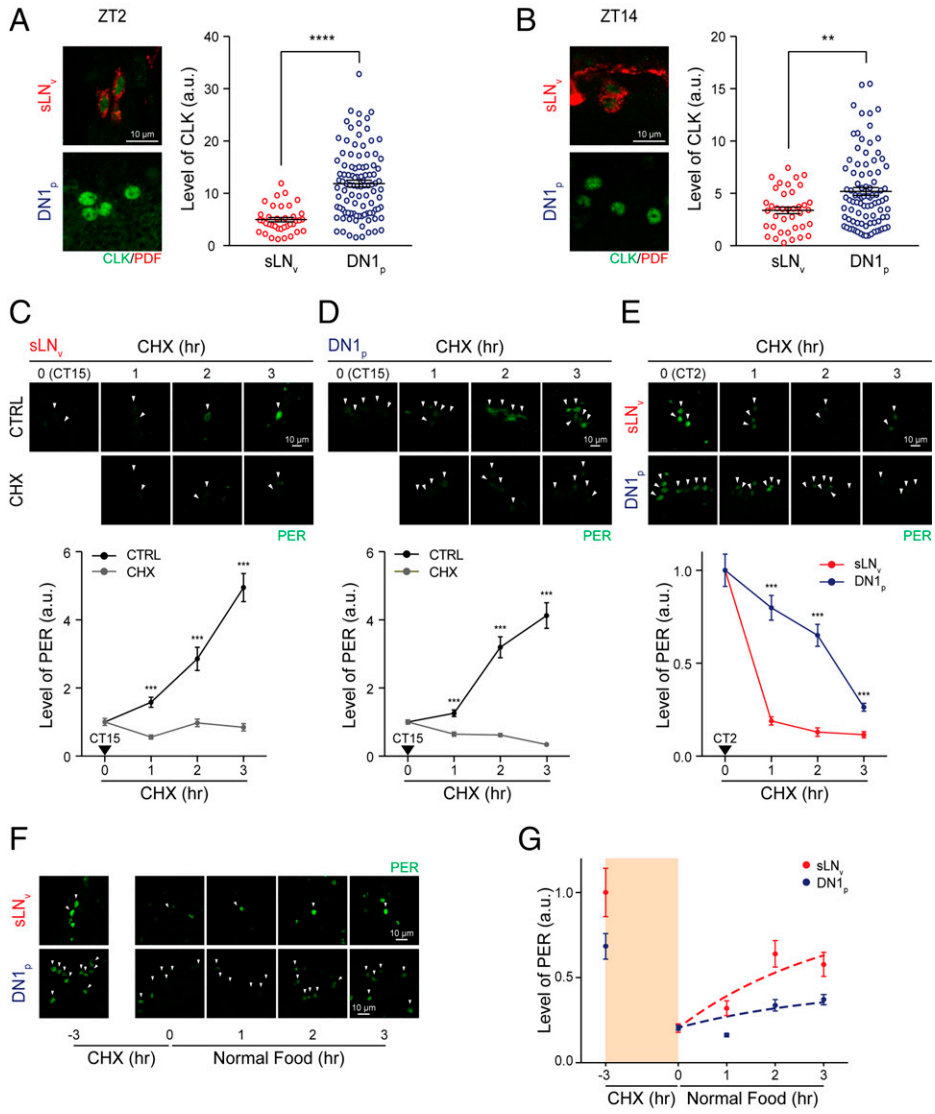

Fig. 3. Levels of CLK and PER degradation and synthesis rates are different between sLN$_v$s and DN1$_p$s. (*A* and *B*) (*Left*) *Clk*-WT flies were collected at ZT2 (*A*) or ZT14 (*B*), and isolated brains were processed for whole-mount immunohistochemistry for CLK (green) and PDF (red). PDF staining was used to mark LN$_v$s. Images are representative for each subset of pacemaker neurons. (*Right*) The levels of CLK were quantified, and values represent mean ± SEM; n = 38 to 100. Asterisks indicate statistically significant difference between values at each time point (Student's t test; $^{**}P < 0.01$, $^{****}P < 0.001$). (*C*–*E*) (*Top*) *Clk*-WT flies were exposed to vehicle- (CTRL) or CHX-containing food, collected at the indicated time, and processed for whole-mount immunohistochemistry for PER (green). White arrowheads indicate PER-containing pacemaker neurons used for quantification. (*Bottom*) The levels of PER were quantified, and all values were normalized to the values at 0 h. Values represent mean ± SEM; n = 41 to 119. Asterisks indicate a statistically significant difference between values at each time point (Student's t test; $^{***}P < 0.001$). (*F* and *G*) w*per*^{01};*per*ΔPDBD flies were maintained in CHX-containing food for 3 h and then transferred to normal food. (*F*) Flies were collected at the indicated time and processed for whole-mount immunohistochemistry for PER (green). White arrowheads indicate PER-containing pacemaker neurons used for quantification. (*G*) The levels of PER were quantified, and values represent mean ± SEM; n = 19 to 80. The orange background represents the CHX exposure period, and dashed lines are fitted curves.

accumulation was faster in sLN$_v$s than DN1$_p$s (Fig. 3 *F* and *G*). These results indicate that PER synthesis is indeed much more efficient in sLN$_v$s than DN1$_p$s, as our model predicted.

Light Perturbation Causes Phase Dispersion in sLN$_v$s before Their Reentrainment. With our combined theoretical and experimental approach, we have identified differences in the molecular clockworks between sLN$_v$s and DN1$_p$s that underlie the differential effects on rhythm caused by the *Clk*-Δ mutation (Figs. 2 and 3). This raised the question of whether these distinct molecular clockworks of sLN$_v$s are critical for their ability to act as the master pacemaker. Thus, we compared the LN and DN models under a regular standard 12:12 LD cycle and under a 4-h phase advance to represent an environmental perturbation (Fig. 4 *A* and *B*). For this, after choosing a single parameter set from the 10^3 parameter sets (Fig. 2*B*), we constructed the groups of the LN and DN models having different phases after LD entrainment (Fig. 4 *A* and *B*, day 0; see *SI Appendix* for details), consistent with experiments (40, 41) wherein sLN$_v$s and DN1$_p$s were shown to have wide ranges of intrinsic phases even after LD entrainment. The constructed groups of LN and DN models have similar phase coherences (i.e., R ≈ 0.8) that were quantified by calculating the mean vector of each peak phase: the length of the vector (R) is 1 or 0 when all the phases are identical or completely incoherent (i.e., evenly spaced), respectively.

However, after the 4-h phase advance (Fig. 4 *A* and *B*, triangle), the LN and DN models showed different phase

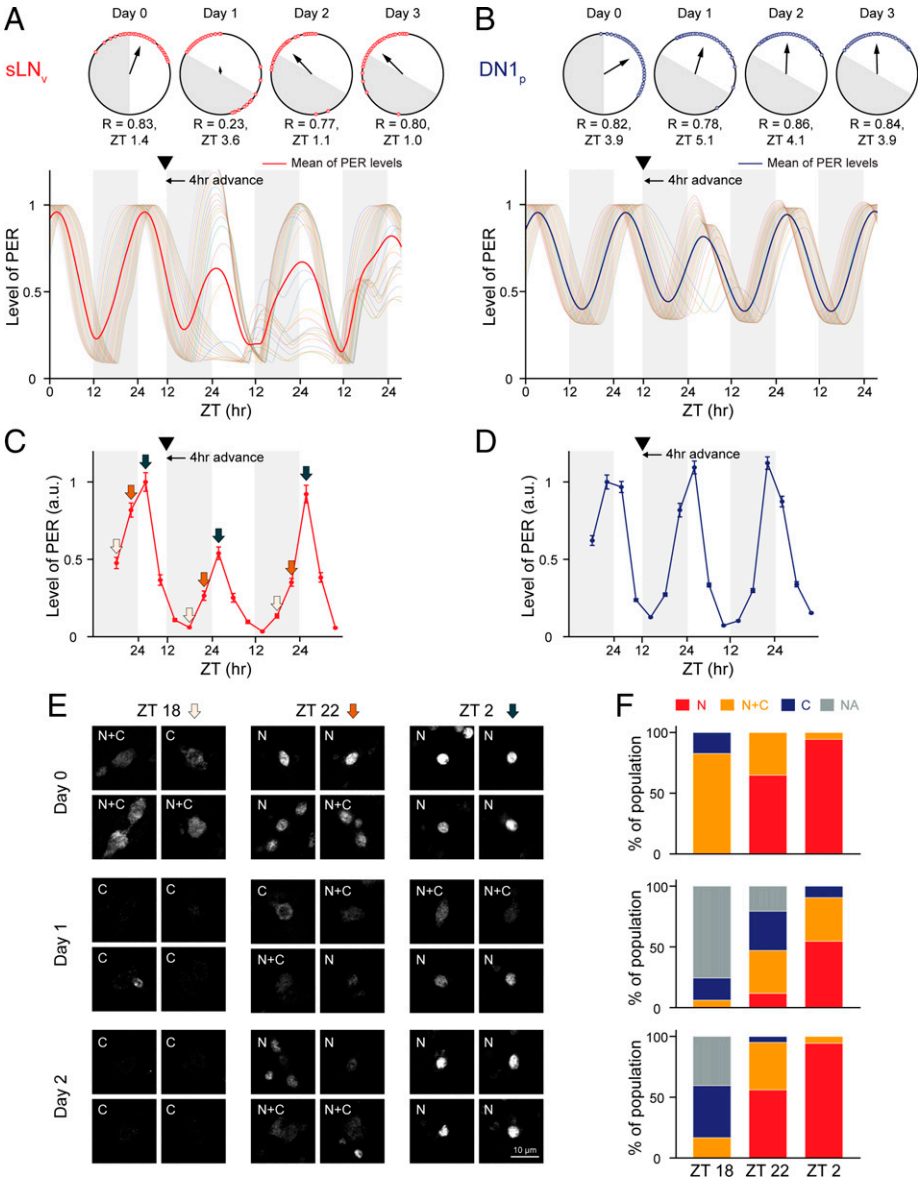

Fig. 4. In response to a phase advance of the LD cycle, sLN$_v$s, but not DN1$_p$s, exhibit phase dispersion. (*A* and *B*) The simulated time series of PER of the LN and DN models in response to a 4-h phase advance (triangle). For each day, peak phases of the LN and DN models are shown in upper circular plots where the arrows of circular plots represent the mean vector of the peak phases. The length R and direction of the mean vector represent the phase coherence and mean phase of the population of oscillators, respectively. On day 0, both the LN and DN models show similar phase coherences. After the phase advance (triangle), the phase coherence of the LN models, but not the DN models, was greatly reduced (day 1). On day 2, the mean phases of both the LN and DN models were nearly reentrained to the advanced LD cycle (*A* and *B*, day 2). Here, time series of PER of the LN and DN models were simulated with the first parameter set (Dataset S1), and white and gray backgrounds represent the L and D conditions, respectively. (*C*–*F*) *Clk*-WT flies were entrained under 12:12 LD for three days and exposed to 4-h phase advance on the evening of the fourth day (day 1). Flies were collected at the indicated time before (day 0), during (day 1), and after (day 2) the phase shift. The levels of PER in sLN$_v$s (*C*) and DN1$_p$s (*D*) were quantified, and values represent mean intensity ± SEM; n = 34 to 54. (*E*) Four representative images of sLN$_v$s PER (white) at the indicated time from day 0 to day 2 are shown. C, cytoplasm; N+C, nucleus + cytoplasm; N, nucleus. (*F*) The percentage of subcellular localization of PER. NA indicated sLN$_v$s with little PER.

coherences. Specifically, the simulated PER rhythms with the LN model exhibited rapid phase dispersion, and thus, their phase coherence was dramatically reduced (R ≈ 0.2; Fig. 4*A*, day 1). In contrast, the simulated PER rhythms with the DN model maintained the phase coherence (R ≈ 0.8; Fig. 4*B*, day 1). Due to the phase dispersion, the mean amplitude of the LN model was greatly reduced compared to that of the DN model (Fig. 4 *A* and *B*, day 1). As a result, the mean amplitude of the LN model was not recovered on day 2, in contrast to the DN model (Fig. 4 *A* and *B*, day 2). Nevertheless, the mean phases of both of the LN and DN models were reentrained to the advanced LD cycle on the same day (Fig. 4 *A* and *B*, days 2 and 3). When different parameter sets among the 10^3 parameter sets were used for the LN model, similarly, the phase dispersion occurred right after the phase advance of the LD cycle, and then the rapid reentrainment was followed for the majority of cases (*SI Appendix*, Fig. S6). Interestingly, for a few cases in which phase dispersion did not occur right after the phase advance of the LD cycle, it took longer for the LN model to be reentrained (*SI Appendix*, Fig. S7). Previous in vivo PER bioluminescence reporter–recording experiments also showed that the mean phase of sLN$_v$s is abruptly shifted to the final phase after strong phase dispersion of sLN$_v$s in response to a phase-advancing light pulse (40, 41) and phase shift (42).

Next, we also examined whether PER rhythms of sLN_vs and $DN1_ps$ exhibited different responses following phase shift as the in silico model predicted. *Clk*-WT flies were entrained under a 12:12 LD cycle and then exposed to the 4-h advanced LD cycle. PER rhythms of sLN_vs and $DN1_ps$ were probed from day 0 (before phase shift) to day 2 (after phase shift) (Fig. 4 *C* and *D*). The trajectory of PER rhythms of sLN_vs and $DN1_ps$ were very similar to those of in silico LN and DN models. In sLN_vs, the mean amplitude of PER rhythms was greatly reduced during phase shift on day 1 and restored, but not fully, after phase shift on day 2 (Fig. 4*C*). In $DN1_ps$, the mean amplitude of PER rhythms was maintained from day 0 to day 2 (Fig. 4*D*). In addition, heterogeneity of the subcellular localization of PER arose in sLN_vs during phase shift (Fig. 4*E*). The subcellular localization can be a phase mark because the nuclear entry of PER is temporally gated for circadian timekeeping (43, 44). Before phase shift (Fig. 4 *E* and *F*, day 0), PER transitions from mostly both cytoplasmic and nuclear localization at early night (e.g., ZT18) to mostly nuclear localization at late night (e.g., ZT22) were followed by exclusively nuclear localization at early day (e.g., ZT2), consistent with previous reports (43, 44). However, at subjectives ZT22 and ZT2 after phase shift (Fig. 4 *E* and *F*, day 1), the population of cytoplasmic, both cytoplasmic and nuclear localization was increased compared to day 0. In addition, neurons with little PER, such that the localization could not be scored, were observed as well. Furthermore, on day 2, the subcellular distribution of PER became similar to that on day 1 (Fig. 4 *E* and *F*). These results indicate that phase coherence was reduced in sLN_vs after phase shift and then restored, as the in silico model predicted.

Our simulation results suggest that such phase dispersion of sLN_vs appears to stem from their distinguishing TTFL from $DN1_ps$. Specifically because PER in the LN model is synthesized and degraded at higher rates compared to PER in the DN model (Fig. 2 *C* and *D*), the level of *per* mRNA in the LN model rapidly increases and decreases during a shorter duration, like a spike (*SI Appendix*, Fig. S8 *A* and *B*). As the phase of a spike-like oscillator is known to be sensitively shifted depending on the time at which the light is perturbed (45), phases of simulated PER rhythms with the LN model are largely dispersed by phase shift, unlike that with the DN model. Whether the distinct TTFL of sLN_vs from $DN1_ps$ indeed contributes to the phase dispersion needs future experimental work.

Discussion

In the *Drosophila* circadian clock, some molecular differences in pacemaker neurons have been reported (46–49) in addition to their different repertoire of transcripts (50–53). However, it has been poorly understood whether and why key molecular mechanisms for generating circadian rhythms differ among pacemaker neurons. In this study, we found differences between the core TTFL of the circadian clock in sLN_vs and $DN1_ps$ by using a combination of theoretical and experimental approaches. Furthermore, we found that such distinct characteristics of the core TTFL in sLN_vs enables them to generate strong rhythms while flexibly adapting their phase upon changes to the environmental lighting conditions.

To understand why PER rhythms are altered differently by the same *Clk*-Δ mutation between sLN_vs and $DN1_ps$, we developed a systematic modeling approach (Fig. 2*A* and *SI Appendix*, Fig. S2). That is, we investigated all possible differences in the core TTFL of sLN_vs and $DN1_ps$ to identify key differences that explain their different alterations by the *Clk*-Δ mutation. This allowed us to identify the 10^3 parameter sets of mathematical models that can reproduce different time series of PER between sLN_vs and $DN1_ps$ (Fig. 2*B* and *SI Appendix*, Fig. S3). Then, by analyzing the common patterns of the 10^3 parameter sets (Fig. 2*C*), we were able to identify key differences in molecular clockworks between sLN_vs and $DN1_ps$: higher synthesis and turnover of PER and lower CLK levels in sLN_vs than $DN1_ps$ (Fig. 2 *C* and *D*). While we assumed that the dissociation constants are the same to avoid the identifiability issue of the parameter estimation, the dissociation constants could also differ in molecular clockworks between sLN_vs and $DN1_ps$ (54). Investigating this will be interesting in future work.

We analyzed the patterns of 10^3 parameter sets rather than a single best-fit parameter set to avoid overfitting, because the best-fit parameter may not yield the most meaningful parameters when models contain a large number of parameters (55). Such a systematic approach has also been successfully used to resolve the unexpected dynamics in biological systems (56–58). While these previous studies focused on identification of hidden regulation underlying a single system, we investigated the difference between two systems, sLN_vs and $DN1_ps$. Thus, we used the regularization cost, penalizing the difference in the values of parameters between the LN and DN models, to avoid unnecessary differences (*SI Appendix*, Fig. S2 B and D). This systematic modeling framework is expandable to identify heterogeneity of other systems.

The predicted lower CLK levels in sLN_vs than in $DN1_ps$ were confirmed by in vivo experiments (Fig. 3 *A* and *B*). Given the lower amount of the transcription factor CLK, one can imagine that de novo–synthesized nascent *per* transcript would be lower, producing a lower amount of PER in sLN_vs than in $DN1_ps$. But PER is more rapidly synthesized in sLN_vs than in $DN1_ps$ (Fig. 3 *F* and *G*), indicating that the production of PER in sLN_vs might be enhanced by posttranscriptional mechanisms. Intriguingly, the translation activation complex of ATX2 and TYF posttranscriptionally regulates *per* mRNA in an LN-specific manner (36–38). miRNAs are also important posttranscriptional regulators of gene expression that degrade target mRNA and/or inhibit its translation. Numerous miRNAs regulate the circadian rhythm by affecting *Clk*, *clockwork orange*, *tim*, or output genes (59–65). While no microRNA (miRNA) targeted toward *per* mRNA has been identified so far, the different repertoire of miRNA in pacemaker neurons might be responsible for the different kinetics of PER accumulation.

In addition, the predicted higher turnover rate of PER in sLN_vs than in $DN1_ps$ was also confirmed by in vivo experiments (Fig. 3 *C*–*E*). What could cause these differences in the degradation rate of PER between sLN_vs and $DN1_ps$? Throughout the day, PER is progressively phosphorylated by several kinases including DBT (casein kinase I ortholog in flies), casein kinase 2 (CK2), NEMO, and Shaggy (GSK3-β ortholog in flies) (47, 66–70). Hyperphosphorylated PER is degraded by the ubiquitin-proteasome system via recognition of Ser47 phosphorylation by the ubiquitin ligase Supernumerary Limbs (SLIMB). Thus, different repertoires of kinase activity in each group of pacemaker neurons might result in different kinetics of PER hyperphosphorylation leading to Ser47 phosphorylation, which is the PER degradation mark. For instance, Ser47 phosphorylation and PER degradation is delayed by NEMO-dependent phosphorylation of the middle part of PER. Intriguingly, NEMO is expressed in sLN_vs, large ventral lateral neurons, dorsal lateral neurons, and DN1s but not in DN2s or DN3s (71). Furthermore, CK2 is expressed only in LN_vs (47, 48). Collectively, we reasoned that a unique repertoire of kinases cooperates to make PER more susceptible to degradation in sLN_vs than in $DN1_ps$. Of course, given that the phosphorylation status of a protein is regulated by phosphatases, the phosphatase repertoire and/or expression level could be another important determinant of degradation rate. Indeed, PP1 and PP2A affected PER phosphorylation and thus its stability (72, 73).

Our mathematical model predicted that the CLK-Δ mutation induced different rhythm alterations in sLN_vs and $DN1_ps$ (Fig. 1) due to the differences in molecular clockworks between sLN_vs and $DN1_ps$ (Fig. 2*D* and *SI Appendix*, Fig. S5). Specifically, when PER levels are higher than CLK levels in the nucleus, the majority of CLK is sequestered and, thus, transcription of *per* mRNA is suppressed (i.e., the suppression phase) (*SI Appendix*, Fig. S5 A–D). As a result, only when PER levels are lower than CLK levels in the nucleus is the transcription of *per* mRNA promoted (i.e., the activation phase). However, as the binding between CLK and PER is disrupted due to the CLK-Δ mutation, even when PER levels are higher than CLK levels, free CLK is available, and thus, the transcription of *per* mRNA is weakly promoted (*SI Appendix*, Fig. S5 B and D; inset). This weak transcription of *per* mRNA dramatically increases PER levels compared to CLK levels due to the high synthesis rate of PER and the low CLK levels in the LN-Δ model (*SI Appendix*, Fig. S5 A and E). As a result, the transcription of *per* mRNA cannot be fully promoted. This disruption of the transition from the suppression phase to the activation phase dampens circadian rhythms in the LN-Δ model. On the other hand, the weak transcription of *per* mRNA has little effect on the ratio between PER levels and CLK levels due to the high CLK levels and low synthesis rate of PER in the DN-Δ model (*SI Appendix*, Fig. S5 C and E). Thus, even in the presence of the CLK-Δ mutation, the transition between the activation and suppression phases occurs, leading to quasi-normal circadian rhythms in the DN-Δ model. Taken together, the LN model shows a greater sensitivity of the transcription in response to the change in the level of PER than the DN model to generate stronger rhythms. However, due to such greater sensitivity, when the system is perturbed (i.e., mutation), the LN model shows a more sensitive response compared to the DN model, leading to the loss of rhythms. As the greater sensitivity is cooperatively generated by the high synthesis rate of PER and low level of CLK (*SI Appendix*, Fig. S5E), the LN-Δ model predicts that changing a single parameter alone (i.e., synthesis rate of PER) will not rescue the rhythms disrupted by the CLK-Δ mutation in sLN_vs (*SI Appendix*, Fig. S9). It would be interesting in future work to investigate whether the disrupted rhythms can be rescued by simultaneously changing multiple parameters of the molecular clockworks in sLN_vs.

Why, then, do sLN_vs have such different molecular properties from $DN1_ps$? Due to the fast synthesis and turnover rates of PER, sLN_vs can generate rhythms with high amplitudes (Fig. 1*E* and *SI Appendix*, Fig. S5), which is critical to yield clear signals to slave oscillators. Unexpectedly, although typically strong oscillators with high amplitudes have difficulty in adapting to environmental changes (e.g., jet lag) (74), we found that sLN_vs can be reentrained to the new LD cycle as rapidly as $DN1_ps$ (Fig. 4). Interestingly, before the reentrainment, unlike $DN1_ps$, the phases of sLN_vs are greatly dispersed. Our in silico study proposes that the phase dispersion stems from the distinct property of TTFL in sLN_vs from $DN1_ps$ due to its spike-like and sensitive transcription yielding strong oscillation (*SI Appendix*, Fig. S8), consistent with ref. 45. Another study also showed that the sensitive response of *per* mRNA in response to the environmental change, yielding phase plasticity, is the feature of robust oscillators (75). That is, the sensitive change of *per* mRNA, and thus sensitive phase shifts under environmental change, counterbalance the change of the other reaction rates and lead to period robustness (75). Taken together, due to the distinct molecular clockworks of sLN_vs compared to those of $DN1_ps$, sLN_vs could obtain both robustness (i.e., high amplitude and period robustness) and plasticity (i.e., fast entrainment and a wide range of entrainment), which are critical characteristics for a master pacemaker.

Materials and Methods

Fly Strains. The following *Drosophila* strains were used in this study: p{*dClk*-WT}; Clk^{out} (27), p{*Clk*-Δ};Clk^{out} flies (27), and $w per^{01}$;*per*ΔPDBD (39).

Immunohistochemistry and Image Analysis. Adult fly heads were cut in ice-cold Schneider's *Drosophila* media (SM), and ∼10 brains were analyzed for each time point. Heads were fixed in 4% formaldehyde and washed with 0.5% PAXD buffer (1× phosphate buffered saline [PBS], 5% bovine serum albumin, 0.03% sodium deoxycholate, and 0.03% Triton X-100). Fixed heads were dissected, and the isolated brains were permeabilized by incubation in 1% PBT (1× PBS and 1% Triton X-100) for 20 min and then incubated in blocking solution (PAXD containing 5% horse serum). Primary antibodies were added directly to the blocking solution, and brains were incubated overnight at 4 °C. The following primary antibodies and final dilutions were used: anti-PER antibody (Rb1), 1:100 (44) and anti-PDF antibody (C7), 1:200 (Developmental Studies Hybridoma Bank). The brains were washed with PAXD buffer and incubated overnight at 4 °C with secondary antibodies in blocking solution. Alexa Fluor 488–conjugated anti-rabbit IgG (Invitrogen) and Alexa Fluor 555–conjugated anti-mouse IgG (Invitrogen) were used at a final dilution of 1:200. Samples were washed several times with PAXD, incubated in 0.1 M phosphate buffer containing 50% glycerol for 15 to 30 min, and mounted using Vectashield (Vector Laboratories). Confocal images were obtained with an LSM800 confocal microscope (Carl Zeiss) and processed with ZEN software (Carl Zeiss). Scoring of staining intensities was performed on single optical sections that show the maximum sectional area for each neuron. For each neuron, area and mean intensity were obtained using ImageJ software (NIH). The background staining level was measured in the field surrounding each neuronal group and subtracted from the mean intensities measured for the cells. The level of PER was quantified by obtaining the relative concentration of PER in the whole cell, the variable of the mathematical model, for the fitting of the model (Fig. 2 *A* and *B*). Since the concentration is defined by total amount divided by volume, we first calculated the sum intensity of PER protein to represent the total amount of PER protein by multiplying the mean intensity and spherical volume estimated from the PER-stained area (Fig. 1 *C* and *E*). The same volume was used, since we found that sLN_vs and $DN1_ps$ have similar areas. Therefore, the sum intensity of PER is equivalent to the relative concentration of PER. We calculated the amplitudes of PER rhythms as the difference between the maximum and minimum average intensities. To compare the amplitude of PER rhythms of *Clk*-Δ flies with that of *Clk*-WT flies, the relative amplitude was calculated by dividing each amplitude of PER rhythms of *Clk*-WT flies and *Clk*-Δ flies by that of *Clk*-WT flies so that the relative amplitude of PER rhythms of *Clk*-WT flies is one.

Likelihood Ratio Test for Detecting Rhythmicity. We used the log-likelihood ratio (LR) test to detect the rhythmicity of the short time-series data (Fig. 1 *C* and *E* and *SI Appendix*, Table S1) because the method yields a low false-positive error (76). We used the significance criteria ($P < 0.01$) suggested by ref. 76. This calculation was done using the R package diffCircadian provided by Ding et al. The R package diffCircadian is available at https://rdrr.io/github/diffCircadian/diffCircadian/.

CHX Treatment. To score the degradation rate of PER, *Clk*-WT flies were fed with the protein synthesis inhibitor CHX (Sigma-Aldrich No. C7698) dissolved into sweet food (20% sucrose and 2% agar). The flies were exposed to 4 d of 12:12 LD at 25 °C and subsequently kept in DD for 4 d. At the fourth day in DD, before transferring the flies into the vehicle- or CHX-containing food, the flies were starved for 3 h to promote feeding. The flies were maintained in CHX-containing food and collected at the indicated time and processed for brain immunostaining with PER. To assess the synthesis rate of PER, $w per^{01}$;*per*ΔPDBD flies were treated with CHX as above. After 3 h of CHX incubation, flies were transferred to normal food, collected at the indicated time, and processed for brain immunostaining with PER.

Systematic Modeling Approach to Identify the Differences in the Core TTFL between sLN_vs and $DN1_ps$. To identify the differences in molecular clockworks between sLN_vs and $DN1_ps$, we developed a mathematical model that describes the core TTFL of the circadian clock in *Drosophila* using ordinary differential equations based on mass action kinetics (Fig. 2*A*; see *SI Appendix* for details). This mathematical model explicitly describes stoichiometric bindings between the key regulators of *per* transcription, PER, CLK, and E-box of the *per* promoter. To reduce the number of parameters and thus avoid the unidentifiability of parameter estimation, we nondimensionalized the model and simplified the model by using the total quasi–steady-state approximation, which is known to accurately reduce models with stoichiometric protein–protein interactions (77) (see *SI Appendix* for details). Then, we used two different

parameter sets to construct the LN and DN models, describing the core TTFL of sLN_vs and $DN1_ps$, respectively. Furthermore, we replaced CLK-WT with CLK-Δ in the models by modifying the parameters describing molecular properties of CLK to develop the LN-Δ and DN-Δ models.

The parameters of the four models (*SI Appendix*, Tables S2 and S3) were estimated by fitting them to the experimentally measured time series of PER with the SA method. To accelerate the parameter estimation, we performed the estimation in four steps (see *SI Appendix*, Fig. S2 for details) and weighted each term of the fitting cost by its own value so that more weight was given to the cost when it was larger. Importantly, to avoid unnecessary parameter differences between the LN and DN models, we used a regularization cost, giving a penalty for differences in the parameters of the LN and DN models.

This process was repeated until 10^3 successful parameter sets, with which the four models can accurately reproduce experimentally measured time series (Fig. 2*B*), were obtained. Then, the common patterns of the 10^3 parameter sets were analyzed to identify key differences in molecular clockworks between the LN and DN models (Fig. 2 *C* and *D*). This systematic modeling approach allowed us to avoid overfitting of the models caused by a large number of parameters. More detailed information about a systematic modeling approach is available in *SI Appendix*.

Data Availability. All study data are included in the article and/or supporting information. The Matlabcodes for the mathematical model and its parameter estimation are available at https://github.com/Mathbiomed/SA_Drosophila_Clock.

ACKNOWLEDGMENTS. This work was supported by National Research Foundation of Korea, Ministry of Science, and ICT grant nos. NRF- 2017R1A2B2010334 (E.Y.K.), NRF-2019R1A5A2026045 (E.Y.K.), NRF-2020R1A2C2007158 (E.Y.K.), and NRF-2016 RICIB 3008468 (J.K.K.), Human Frontiers Science Program Organization Grant RGY0063/2017 (J.K.K.), and Institute for Basic Science Grant BS-R029-C3 (J.K.K.). We also thank Boseung Choi for discussing statistical analysis and Life Science Editors for editing support.

1. A. Eskin, Identification and physiology of circadian pacemakers. Introduction. *Fed. Proc.* **38**, 2570–2572 (1979).
2. U. Albrecht, Timing to perfection: The biology of central and peripheral circadian clocks. *Neuron* **74**, 246–260 (2012).
3. C. S. Pittendrigh, Temporal organization: Reflections of a Darwinian clock-watcher. *Annu. Rev. Physiol.* **55**, 16–54 (1993).
4. S. Honma, The mammalian circadian system: A hierarchical multi-oscillator structure for generating circadian rhythm. *J. Physiol. Sci.* **68**, 207–219 (2018).
5. D. Stoleru, Y. Peng, P. Nawathean, M. Rosbash, A resetting signal between *Drosophila* pacemakers synchronizes morning and evening activity. *Nature* **438**, 238–242 (2005).
6. C. Hermann-Luibl, C. Helfrich-Förster, Clock network in *Drosophila*. *Curr. Opin. Insect Sci.* **7**, 65–70 (2015).
7. D. Stoleru, Y. Peng, J. Agosto, M. Rosbash, Coupled oscillators control morning and evening locomotor behaviour of *Drosophila*. *Nature* **431**, 862–868 (2004).
8. B. Grima, E. Chélot, R. Xia, F. Rouyer, Morning and evening peaks of activity rely on different clock neurons of the *Drosophila* brain. *Nature* **431**, 869–873 (2004).
9. D. Stoleru *et al.*, The *Drosophila* circadian network is a seasonal timer. *Cell* **129**, 207–219 (2007).
10. F. Guo, I. Cerullo, X. Chen, M. Rosbash, PDF neuron firing phase-shifts key circadian activity neurons in *Drosophila*. *eLife* **3**, e02780 (2014).
11. M. Schlichting *et al.*, A neural network underlying circadian entrainment and photoperiodic adjustment of sleep and activity in *Drosophila*. *J. Neurosci.* **36**, 9084–9096 (2016).
12. M. T. Li *et al.*, Hub-organized parallel circuits of central circadian pacemaker neurons for visual photoentrainment in *Drosophila*. *Nat. Commun.* **9**, 4247 (2018).
13. S. Veleri, C. Brandes, C. Helfrich-Förster, J. C. Hall, R. Stanewsky, A self-sustaining, light-entrainable circadian oscillator in the *Drosophila* brain. *Curr. Biol.* **13**, 1758–1767 (2003).
14. A. Klarsfeld *et al.*, Novel features of cryptochrome-mediated photoreception in the brain circadian clock of *Drosophila*. *J. Neurosci.* **24**, 1468–1477 (2004).
15. T. Yoshii *et al.*, The neuropeptide pigment-dispersing factor adjusts period and phase of *Drosophila's* clock. *J. Neurosci.* **29**, 2597–2610 (2009).
16. A. Chatterjee *et al.*, Reconfiguration of a multi-oscillator network by light in the *Drosophila* circadian clock. *Curr. Biol.* **28**, 2007–2017.e4 (2018).
17. D. J. Cavanaugh *et al.*, Identification of a circadian output circuit for rest:activity rhythms in *Drosophila*. *Cell* **157**, 689–701 (2014).
18. F. Guo, M. Holla, M. M. Díaz, M. Rosbash, A circadian output circuit controls sleep-wake arousal in *Drosophila*. *Neuron* **100**, 624–635.e4 (2018).
19. F. Guo *et al.*, Circadian neuron feedback controls the *Drosophila* sleep—Activity profile. *Nature* **536**, 292–297 (2016).
20. J. D. Ni *et al.*, Differential regulation of the *Drosophila* sleep homeostat by circadian and arousal inputs. *eLife* **8**, e40487 (2019).
21. A. Lamaze, P. Krätschmer, K. F. Chen, S. Lowe, J. E. C. Jepson, A wake-promoting circadian output circuit in *Drosophila*. *Curr. Biol.* **28**, 3098–3105.e3 (2018).
22. A. F. Barber, R. Erion, T. C. Holmes, A. Sehgal, Circadian and feeding cues integrate to drive rhythms of physiology in *Drosophila* insulin-producing cells. *Genes Dev.* **30**, 2596–2606 (2016).
23. A. Murad, M. Emery-Le, P. Emery, A subset of dorsal neurons modulates circadian behavior and light responses in *Drosophila*. *Neuron* **53**, 689–701 (2007).
24. R. V. M. de Azevedo, C. Hansen, K. F. Chen, E. Rosato, C. P. Kyriacou, Disrupted glutamate signaling in *Drosophila* generates locomotor rhythms in constant light. *Front. Physiol.* **11**, 145 (2020).
25. P. E. Hardin, Molecular genetic analysis of circadian timekeeping in *Drosophila*. *Adv. Genet.* **74**, 141–173 (2011).
26. A. Patke, M. W. Young, S. Axelrod, Molecular mechanisms and physiological importance of circadian rhythms. *Nat. Rev. Mol. Cell Biol.* **21**, 67–84 (2020).
27. E. Lee *et al.*, Pacemaker-neuron-dependent disturbance of the molecular clockwork by a *Drosophila* CLOCK mutant homologous to the mouse Clock mutation. *Proc. Natl. Acad. Sci. U.S.A.* **113**, E4904–E4913 (2016).
28. K. Shimomura *et al.*, Usf1, a suppressor of the circadian Clock mutant, reveals the nature of the DNA-binding of the CLOCK:BMAL1 complex in mice. *eLife* **2**, e00426 (2013).
29. M. P. Myers, K. Wager-Smith, A. Rothenfluh-Hilfiker, M. W. Young, Light-induced degradation of TIMELESS and entrainment of the *Drosophila* circadian clock. *Science* **271**, 1736–1740 (1996).
30. B. Kloss, A. Rothenfluh, M. W. Young, L. Saez, Phosphorylation of period is influenced by cycling physical associations of double-time, period, and timeless in the *Drosophila* clock. *Neuron* **30**, 699–706 (2001).
31. P. Smolen, P. E. Hardin, B. S. Lo, D. A. Baxter, J. H. Byrne, Simulation of Drosophila circadian oscillations, mutations, and light responses by a model with VRI, PDP-1, and CLK. *Biophys. J.* **86**, 2786–2802 (2004).
32. S. Risau-Gusman, P. M. Gleiser, A mathematical model of communication between groups of circadian neurons in *Drosophila melanogaster*. *J. Biol. Rhythms* **29**, 401–410 (2014).
33. S. Lück, K. Thurley, P. F. Thaben, P. O. Westermark, Rhythmic degradation explains and unifies circadian transcriptome and proteome data. *Cell Rep.* **9**, 741–751 (2014).
34. J. K. Kim, D. B. Forger, A mechanism for robust circadian timekeeping via stoichiometric balance. *Mol. Syst. Biol.* **8**, 630 (2012).
35. J. K. Kim, Protein sequestration versus Hill-type repression in circadian clock models. *IET Syst. Biol.* **10**, 125–135 (2016).
36. C. Lim, R. Allada, ATAXIN-2 activates PERIOD translation to sustain circadian rhythms in *Drosophila*. *Science* **340**, 875–879 (2013).
37. C. Lim *et al.*, The novel gene twenty-four defines a critical translational step in the *Drosophila* clock. *Nature* **470**, 399–403 (2011).
38. Y. Zhang, J. Ling, C. Yuan, R. Dubruille, P. Emery, A role for *Drosophila* ATX2 in activation of PER translation and circadian behavior. *Science* **340**, 879–882 (2013).
39. E. Y. Kim, H. W. Ko, W. Yu, P. E. Hardin, I. Edery, A DOUBLETIME kinase binding domain on the *Drosophila* PERIOD protein is essential for its hyperphosphorylation, transcriptional repression, and circadian clock function. *Mol. Cell. Biol.* **27**, 5014–5028 (2007).
40. L. Roberts, T. L. Leise, D. K. Welsh, T. C. Holmes, Functional contributions of strong and weak cellular oscillators to synchrony and light-shifted phase dynamics. *J. Biol. Rhythms* **31**, 337–351 (2016).
41. L. Roberts *et al.*, Light evokes rapid circadian network oscillator desynchrony followed by gradual phase retuning of synchrony. *Curr. Biol.* **25**, 858–867 (2015).
42. C. Nave *et al.*, Weekend light shifts evoke persistent *Drosophila* circadian neural network desynchrony. *J. Neurosci.* **41**, 5173–5189 (2021).
43. K. D. Curtin, Z. J. Huang, M. Rosbash, Temporally regulated nuclear entry of the *Drosophila* period protein contributes to the circadian clock. *Neuron* **14**, 365–372 (1995).
44. E. Y. Kim *et al.*, A role for O-GlcNAcylation in setting circadian clock speed. *Genes Dev.* **26**, 490–502 (2012).
45. A. E. Granada, H. Herzel, How to achieve fast entrainment? The timescale to synchronization. *PLoS One* **4**, e7057 (2009).
46. D. Top, M. W. Young, Coordination between differentially regulated circadian clocks generates rhythmic behavior. *Cold Spring Harb. Perspect. Biol.* **10**, a033589 (2018).
47. J. M. Lin *et al.*, A role for casein kinase 2alpha in the *Drosophila* circadian clock. *Nature* **420**, 816–820 (2002).
48. D. Top, E. Harms, S. Syed, E. L. Adams, L. Saez, GSK-3 and CK2 kinases converge on timeless to regulate the master clock. *Cell Rep.* **16**, 357–367 (2016).
49. X. Liang, T. E. Holy, P. H. Taghert, Synchronous *Drosophila* circadian pacemakers display nonsynchronous Ca^{2+} rhythms in vivo. *Science* **351**, 976–981 (2016).
50. D. Ma *et al.*, A transcriptomic taxonomy of *Drosophila* circadian neurons around the clock. *eLife* **10**, e63056 (2021).
51. K. C. Abruzzi *et al.*, RNA-seq analysis of *Drosophila* clock and non-clock neurons reveals neuron-specific cycling and novel candidate neuropeptides. *PLoS Genet.* **13**, e1006613 (2017).
52. E. Kula-Eversole *et al.*, Surprising gene expression patterns within and between PDF-containing circadian neurons in *Drosophila*. *Proc. Natl. Acad. Sci. U.S.A.* **107**, 13497–13502 (2010).
53. E. Nagoshi *et al.*, Dissecting differential gene expression within the circadian neuronal circuit of *Drosophila*. *Nat. Neurosci.* **13**, 60–68 (2010).
54. J. R. Beytebiere *et al.*, Tissue-specific BMAL1 cistromes reveal that rhythmic transcription is associated with rhythmic enhancer-enhancer interactions. *Genes Dev.* **33**, 294–309 (2019).

55. J. Lever, M. Krzywinski, N. Altman, Points of significance. Model selection and overfitting. *Nat. Methods* **13**, 703–704 (2016).
56. T. Gotoh *et al.*, Model-driven experimental approach reveals the complex regulatory distribution of p53 by the circadian factor Period 2. *Proc. Natl. Acad. Sci. U.S.A.* **113**, 13516–13521 (2016).
57. A. Ali *et al.*, Rheostatic control of ABA signaling through HOS15-mediated OST1 degradation. *Mol. Plant* **12**, 1447–1462 (2019).
58. X. Zou *et al.*, A systems biology approach identifies hidden regulatory connections between the circadian and cell-cycle checkpoints. *Front. Physiol.* **11**, 327 (2020).
59. S. Kadener *et al.*, A role for microRNAs in the *Drosophila* circadian clock. *Genes Dev.* **23**, 2179–2191 (2009).
60. W. Luo, A. Sehgal, Regulation of circadian behavioral output via a MicroRNA-JAK/STAT circuit. *Cell* **148**, 765–779 (2012).
61. W. Chen *et al.*, Regulation of *Drosophila* circadian rhythms by miRNA let-7 is mediated by a regulatory cycle. *Nat. Commun.* **5**, 5549 (2014).
62. X. Chen, M. Rosbash, mir-276a strengthens *Drosophila* circadian rhythms by regulating timeless expression. *Proc. Natl. Acad. Sci. U.S.A.* **113**, E2965–E2972 (2016).
63. X. Chen, M. Rosbash, MicroRNA-92a is a circadian modulator of neuronal excitability in *Drosophila*. *Nat. Commun.* **8**, 14707 (2017).
64. D. L. Garaulet *et al.*, miR-124 regulates diverse aspects of rhythmic behavior in *Drosophila*. *J. Neurosci.* **36**, 3414–3421 (2016).
65. X. Xia *et al.*, Regulation of circadian rhythm and sleep by miR-375-timeless interaction in *Drosophila*. *FASEB J.* **34**, 16536–16551 (2020).
66. J. L. Price *et al.*, double-time is a novel *Drosophila* clock gene that regulates PERIOD protein accumulation. *Cell* **94**, 83–95 (1998).
67. B. Akten *et al.*, A role for CK2 in the *Drosophila* circadian oscillator. *Nat. Neurosci.* **6**, 251–257 (2003).
68. J. M. Lin, A. Schroeder, R. Allada, In vivo circadian function of casein kinase 2 phosphorylation sites in *Drosophila* PERIOD. *J. Neurosci.* **25**, 11175–11183 (2005).
69. J. C. Chiu, H. W. Ko, I. Edery, NEMO/NLK phosphorylates PERIOD to initiate a time-delay phosphorylation circuit that sets circadian clock speed. *Cell* **145**, 357–370 (2011).
70. H. W. Ko *et al.*, A hierarchical phosphorylation cascade that regulates the timing of PERIOD nuclear entry reveals novel roles for proline-directed kinases and GSK-3beta/SGG in circadian clocks. *J. Neurosci.* **30**, 12664–12675 (2010).
71. W. Yu, J. H. Houl, P. E. Hardin, NEMO kinase contributes to core period determination by slowing the pace of the *Drosophila* circadian oscillator. *Curr. Biol.* **21**, 756–761 (2011).
72. S. Sathyanarayanan, X. Zheng, R. Xiao, A. Sehgal, Posttranslational regulation of *Drosophila* PERIOD protein by protein phosphatase 2A. *Cell* **116**, 603–615 (2004).
73. Y. Xue, J. C. Chiu, Y. Zhang, SUR-8 interacts with PP1-87B to stabilize PERIOD and regulate circadian rhythms in *Drosophila*. *PLoS Genet.* **15**, e1008475 (2019).
74. U. Abraham *et al.*, Coupling governs entrainment range of circadian clocks. *Mol. Syst. Biol.* **6**, 438 (2010).
75. T. S. Hatakeyama, K. Kaneko, Reciprocity between robustness of period and plasticity of phase in biological clocks. *Phys. Rev. Lett.* **115**, 218101 (2015).
76. H. Ding *et al.*, Likelihood-based tests for detecting circadian rhythmicity and differential circadian patterns in transcriptomic applications. *Brief. Bioinform.* **22**, bbab224 (2021).
77. J. K. Kim, J. J. Tyson, Misuse of the Michaelis-Menten rate law for protein interaction networks and its remedy. *PLOS Comput. Biol.* **16**, e1008258 (2020).
78. J. Cohen, *Statistical Power Analysis for the Behavioral Sciences* (Lawrence Erlbaum Associates, Hillsdale, NJ, 1988), p. 46.